Rev. Adv. Mater. Sci. 55 (2018) 26-34

STRESS-DRIVEN MIGRATION OF LOW-ANGLE GRAIN BOUNDARIES NEAR CRACK TIPS IN NANOCOMPOSITES CONTAINING INCOHERENT NANOINCLUSIONS

S.V. Bobylev[1,2] and L.-S.D. Galeeva[1]

[1]Institute of Problems of Mechanical Engineering, Russian Academy of Sciences, Bolshoj 61, Vasil. Ostrov, St. Petersburg, 199178, Russia
[2]Peter the Great St. Petersburg Polytechnic University, St. Petersburg 195251, Russia

Received: June 20, 2018

Abstract. Theoretical model describing stress-driven migration of low-angle grain boundaries (GBs) in the vicinity of growing crack in metal matrix nanocomposites with reinforcing (metallic or ceramic) incoherent nanoinclusions is proposed. Using two-dimensional discrete dislocation dynamics approach profiles of migrating GBs are analytically calculated and critical stress for transition into unstable migration mode is found. It is shown that the presence of crack always promotes stress-driven migration and thus grain growth.

1. INTRODUCTION

The nanoscale and interface effects crucially influence plastic behavior of nanocrystalline (NC) and ultrafine-grained (UFG) bulk materials, ultrathin films, and nanowires showing excellent mechanical properties (see, e.g., [1–10]). It is known that in NC and UFG metallic materials, conventional lattice slip is hampered by large amounts of grain boundaries (GBs), in which case plastic flow often occurs through alternative deformation mechanisms mediated by GBs [5]. The stress-driven athermal migration of GBs is generally recognized as one of the deformation modes effectively operating in NC metals in wide range of their structural parameters [5,11–35]. The stress-driven GB migration leads to grain growth that destroys the NC structure and thus results in degradation of material properties.

In general, thermally activated grain growth is viewed as the main negative factor that can come into play in NC metals during their synthesis and thus destroy their NC structure [5]. To suppress the thermally activated grain growth, several approaches are utilized [36,37]. Among them is the use of nanoinclusions (for example, nanoscale precipitates of the second metallic phase in metallic alloys and second-phase ceramic nanoparticles in metal matrix nanocomposites) as obstacles for GB migration (see, e.g., [5,38,39]). Additionally, nanoinclusions also serve as reinforcing structural elements hindering lattice dislocation slip (see, e.g., [40–42]) and affecting crack growth [43–45].

Recently, theoretical model [46] describing the stress-driven GB migration as a plastic deformation mode in metal matrix nanocomposites containing incoherent reinforcing (ceramic or metallic) nanoinclusions was proposed. This model described the migration of low-angle GBs hindered by the presence of nanoparticles. Its authors found stress characteristics of this migration as well as equilibrium and non-equilibrium GB profiles. At the same time, plastic deformation carried by GB migration is accompanied by crystal rotations and thus can be considered as a partial case of rotational deformation. Following experimental data [47–51], crystal

Corresponding author: S.V. Bobylev, e-mail: bobylev.s@gmail.com

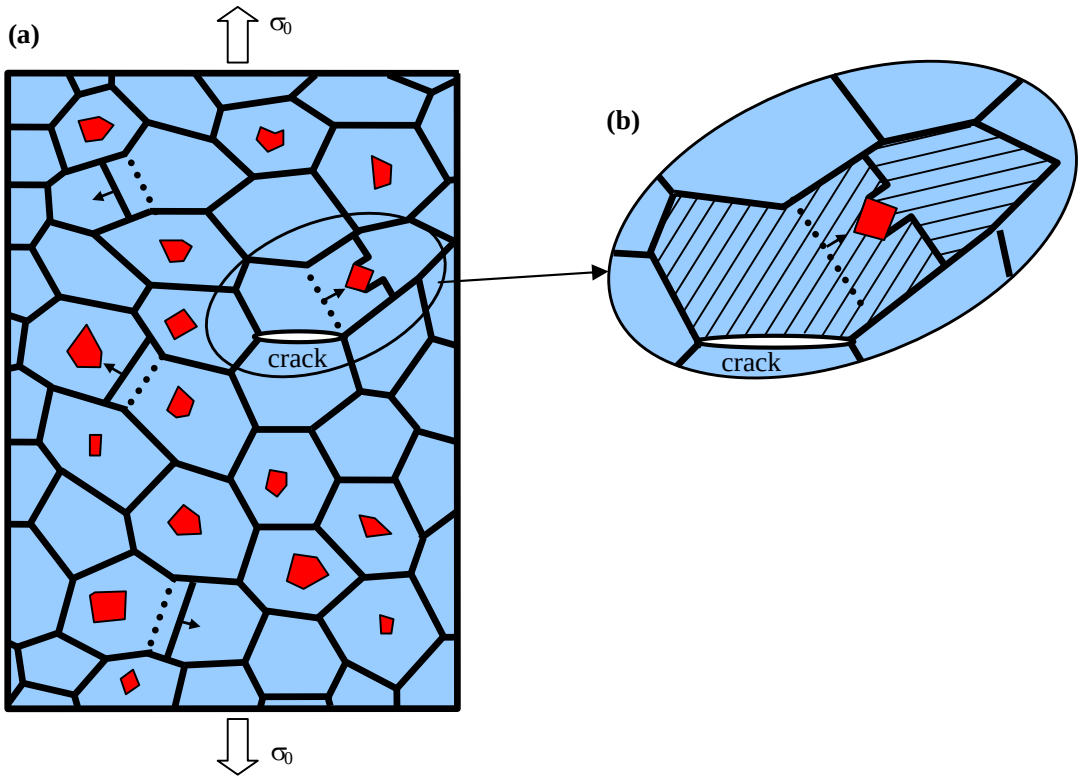

Fig. 1. Stress-driven migration of a grain boundary in a cracked nanocomposite solid containing hard (ceramic or metallic) nanoinclusions inside grains of a metallic matrix. (a) A nanocomposite specimen is under a mechanical load (a two-dimensional general view). (b) The magnified region highlights the state of the nanocomposite, after the stress-driven grain boundary migration.

lattice rotations intensively occur in vicinities of cracks growing in NC and UFG materials. In this context it is highly interesting to understand how presence of cracks affects GB migration in metal matrix nanocomposites containing nanoinclusions. The main aim of this paper is to extend approach developed in Ref. [46] on the case of nanocomposites containing growing cracks. We examine the effects of nanoinclusions on both the critical stresses for the GB migration processes and profiles of migrating GBs.

2. GEOMETRIC ASPECTS OF STRESS-DRIVEN MIGRATION OF LOW-ANGLE GRAIN BOUNDARIES NEAR CRACK TIPS IN NANOCOMPOSITES WITH INCOHERENT NANOINCLUSIONS

Let us consider a nanocomposite sample consisting of an NC metal matrix and incoherent reinforcing (metallic or ceramic) nanoinclusions (Fig. 1). Additionally we assume that there exists an intergranular nanocrack (Fig. 1). For definiteness, we focus our analysis on the situation where the crack is flat, and the sample is under a tensile load σ_0 normal to the crack plane; that is, a mode I cracking (Fig. 1a). The applied load and high stress concentration near the crack tip can induce GB migration near its tip (Fig. 1). For definiteness and simplicity, our consideration will be focused on stress-driven migration of low-angle tilt boundaries conventionally modeled as walls of edge lattice dislocations. Due to the high Peierls barrier for dislocation slip in the ceramic nanoinclusions and the difference in the types of the crystal lattices between the matrix and the metallic nanoinclusions, migrating GBs cannot penetrate them and instead are bent around the incoherent nanoinclusions (Fig. 1b). In doing so, the migrating GBs can either stop at nanoinclusions or move further, depending on the applied load as well as both the geometry and the size of the GBs and nanoinclusions.

In order to calculate the critical parameters at which a migrating GB can bypass a nanoinclusion, we consider a symmetric low-angle tilt boundary terminated at triple junctions A and B in a composite solid in its initial state before the migration (Fig. 2a). Point B is also a location of the crack tip, and GB plane forms angle φ with the normal to the crack

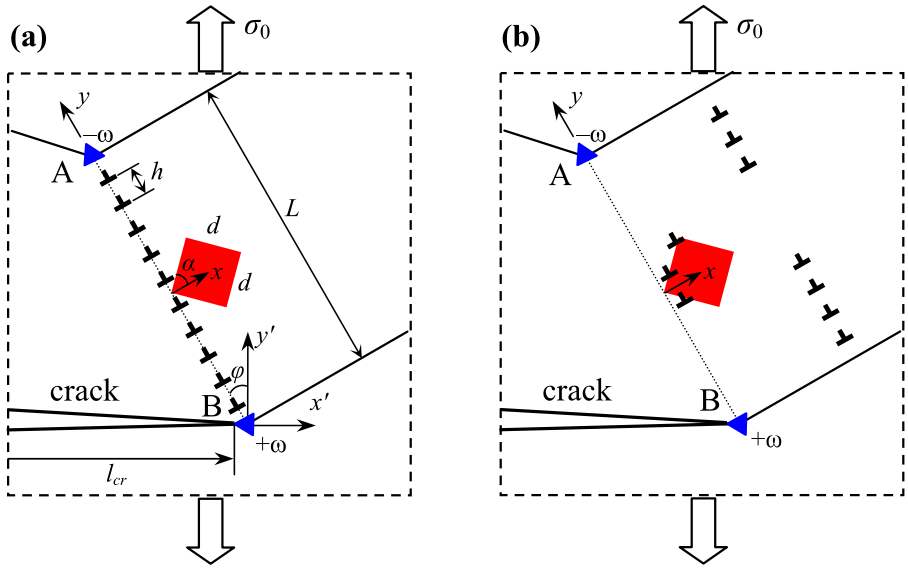

Fig. 2. Migration of a low-angle tilt boundary hindered by an incoherent nanoinclusion impenetrable for dislocations in the vicinity of a crack tip.

plane (load direction). We assume that crack has finite length l_{cr}. In the initial state, in the absence of a mechanical load, the low-angle boundary AB is represented as a straight wall of periodically arranged edge dislocations having the same Burgers vector **b**. The low-angle boundary is characterized by the tilt misorientation angle θ being in the Frank relationship $\sin(\theta/2) = b/(2h)$ [52] with the parameters (period h and Burgers vector magnitude b) of the dislocation wall.

In the initial state before the migration process, other GBs adjacent to the GB AB are assumed to be symmetric tilt boundaries that form the geometrically compensated triple junctions A and B with the boundary AB (Fig. 2a). Following the approach [24,30,32], we do not consider the structure of neighboring GBs and model their stresses by placing wedge disclinations in triple junctions A and B. In doing so, a wedge disclination located at the triple junction A are characterized by the disclination strength $-\omega = -\theta$ and wedge disclination located at the triple junction B and characterized by the disclination strength $\omega = \theta$ (Fig. 2a).

We now consider migration of the GB AB under the applied tensile stress σ_0 affected by the presence of crack in the nanocomposite. This stress is applied normal to the crack plane (mode I cracking) and induces some shear stress τ in dislocation slip planes (see below). When the shear stress τ acts in slip planes of the lattice edge dislocations belonging to the GB AB, these dislocations cooperatively glide from their initial positions (Fig. 2a) to the new positions (Fig. 2b). These stress-driven cooperative displacements of the dislocations result in the migration of the GB AB (Fig. 2b). Similar to the model [46], we assume that the migrating GB is retarded by a wire nanoinclusion having both a square cross section and the long axis normal to the plane of Fig. 2 (and parallel with dislocations lines that form the migrating GB). Within the model, the sides of the square that forms the nanoinclusion cross section have the length d, and one of the square sides makes the angle α with the normal to the GB plane (Fig. 2). Since the inclusion is incoherent, it is assumed to be impenetrable for dislocations that form the dislocation wall. As the main role of the inclusion is in retarding dislocations, we believe that its exact shape is not important.

3. STRESS CHARACTERISTICS AND PROFILE OF A MIGRATING GRAIN BOUNDARY

Let us examine the process of the stress-driven migration of the low-angle GB AB meeting an incoherent nanoinclusion in a metal matrix nanocomposite. In our analysis, we will exploit the methods of the two-dimensional discrete dislocation dynamics approach employed previously for description of the formation, decay or evolution of GBs (see, e.g., [53–56]). Within the approach in question, each dislocation at the low-angle GB AB is under the combined actions of the forces created by the external stress (affected by the presence of the crack), other dislocations belonging to the boundary, and the disclination dipole.

We now calculate these forces and write the corresponding equations for dislocation motion. To do so, we assume that dislocations can move along one slip plane (along the *x*-axis in the coordinate system associated with the GB middle point as shown in Fig. 2), and, therefore, only the projections of the forces on the *x*-axis matter. In these circumstances, the solution of the system of equations, describing one-dimensional motion of dislocations, will be expressed as dependences $x_i(t)$, where x_i is the coordinate of the ith dislocation (i=1,…,N) and t is time. Also, in our examination, in a first approximation, we neglect the difference in the elastic moduli between the nanoinclusions and the matrix and model the nanocomposite as an elastically isotropic, homogeneous solid characterized by the shear modulus G and Poisson's ratio ν.

Within the approach under discussion, the projection F_i of the total force acting on the ith dislocation belonging to the GB AB is written as follows [53]:

$$F_i = b\tau(x_i, y_i) + Db^2 \sum_{\substack{k=1 \\ k\neq i}}^{N} \frac{(x_i - x_k)\left[(x_i - x_k)^2 - (y_i - y_k)^2\right]}{\left[(x_i - x_k)^2 + (y_i - y_k)^2\right]} - Db\omega\left(\frac{x_i(y_i + L/2)}{x_i^2 + (y_i + L/2)^2} - \frac{x_i(y_i - L/2)}{x_i^2 + (y_i - L/2)^2}\right), \quad (1)$$

where D=G/[2π(1-ν)], L denotes the GB length (the distance between the triple junction disclinations that form the dipole (see Fig. 2)), while x_i and y_i=h(i-1/2)-L/2 are the coordinates of the ith dislocation. The first term on the right-hand side of formula (1) describes the force created by the shear stress τ, the second term describes the force of the interaction of the ith dislocation with the other dislocations of the boundary, and the third term describes the force of the interaction of the ith dislocation with the disclination dipole AB. In other words, the third term characterizes the role of GB junctions in the stress-driven GB migration.

Unlike models [46,53,54], where applied shear stress τ was uniform, in the present model the shear stress is perturbed by the presence of a crack and is not uniform anymore. It is known [57] that mode I cracking under the action of applied tensile stress σ_0 produces following stress tensor components in the crack tip vicinity (written in the coordinate system *Ox'y'* with the origin at the crack tip; see Fig. 2a):

$$\sigma_{x'x'} = \frac{K_I}{\sqrt{2\pi r}}\cos(\theta/2)\times\left[1 - \sin(\theta/2)\sin(3\theta/2)\right],$$
$$\sigma_{y'y'} = \frac{K_I}{\sqrt{2\pi r}}\cos(\theta/2)\times\left[1 + \sin(\theta/2)\sin(3\theta/2)\right] + \sigma_0, \quad (2)$$
$$\sigma_{x'y'} = \frac{K_I}{\sqrt{2\pi r}}\sin(\theta/2)\cos(\theta/2)\cos(3\theta/2).$$

Here K_I is the stress intensity factor, r and θ are polar coordinates ($r = \sqrt{x'^2 + y'^2}$, θ = arctan(y'/x')). In the case of finite length crack stress intensity factor can be written as $K_I = \sigma_0\sqrt{\pi l_{cr}/2}$. Using (2) we can write shear stress $\tau = \sigma_{xy}$ by going from coordinate system *Ox'y'* to *Oxy* (see Fig. 2a) using standard formula for tensor components transformation (rotation by angle φ and parallel translation to GB middle point by distance L/2):

$$\tau(x,y) = \sigma_{xy}(x,y) = \cos(2\phi)\sigma_{x'y'}(x',y') + \frac{\sin 2\phi}{2}\left[\sigma_{yy}(x',y') - \sigma_{xx}(x',y')\right],$$

with

$$x' = x\cos\varphi - (y + L/2)\sin\varphi,$$
$$y' = x\sin\varphi + (y + L/2)\cos\varphi. \quad (3)$$

Combining (2) and (3) we find shear stresses τ figuring in formula (1) induced by tensile load σ_0 in dislocation slip planes and perturbed by the presence of a mode I crack.

Now we can write the equations for the motion of dislocations composing the dislocation wall (low-angle tilt boundary) in the following form:

$$m\frac{d^2 x_i}{dt^2} + \beta\frac{dx_i}{dt} = F_i, \quad i = 1,...,N. \quad (4)$$

The first derivatives dx_i/dt in these equations take into account the dislocation motion friction (associated with the dynamic retardation of the crystalline lattice to the dislocation glide), and β is the viscosity coefficient. The dislocation mass m is given by the standard approximation [53] as $m = \rho b^2/2$, where ρ is the material density.

With Eqs. (1)–(4), we simulated the motion of the low-angle tilt boundary AB in the presence of a nanoinclusion. In the simulations, it was assumed that if a dislocation approaches the boundary of the

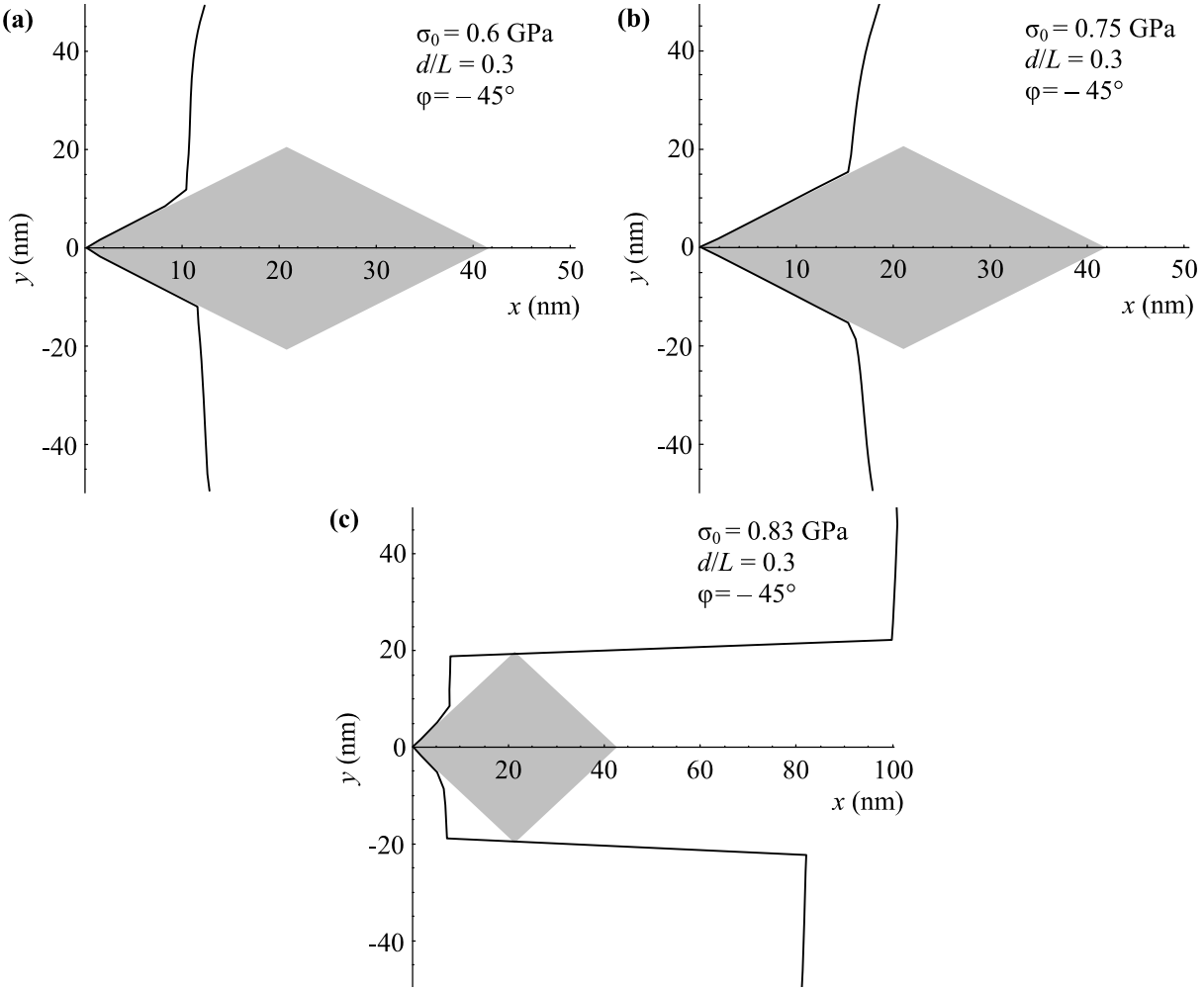

Fig. 3. Geometry of a migrating grain boundary that bends around a nanoinclusion at various values of applied stress calculated for angle φ = -45°. (a), (b) Equilibrium profiles of a migrating grain boundary. (c) Nonequilibrium profile of a migrating grain boundary.

nanoinclusion, it stops. Our analysis has shown that similar to the case of GB migration in single-phase metallic solids [53,54], GB motion in the nanocomposite can occur in two different modes. In the first mode, all the dislocations eventually approach their equilibrium positions, and we refer to this mode as the limited GB migration. In the second mode, some dislocations stop at the nanoinclusion boundary, while others move unrestrictedly far away from it. We define this mode as the unlimited GB migration (Obviously, in reality, the unlimited migration of a GB is eventually stopped when this boundary meets a neighboring GB).

With the calculated positions of the dislocations, we revealed the profiles of the migrating GB AB in various cases. As shear stresses acting in slip planes obviously depend on the angle φ between load direction and GB plane we considered two typical cases corresponding to the maximum values of shear stresses: φ = -45 and φ = 45° (positive values of φ correspond to the counter clockwise rotation of GB plane relative to load direction). Figs. 3 and 4 show these profiles in the case of a composite solid with aluminum matrix, for the following values of parameters: G = 27 GPa, ν = 0.34, b = 0.285 nm, and ρ = 2712 kg·m^{-3}. Also, following [58], we take the value of β as $\beta = 5 \cdot 10^{-5}$ Pa·s as well as put the values of other parameters as follows: $l_{cr} = L$, α = 45°, ω = 5°, and N = 30. The latter number of dislocations at the GB AB corresponds to the GB length of $L \approx 100$ nm.

Figs. 3a and 3b present the simulated equilibrium profiles of the migrating GB, for d/L = 0.3, φ = -45° and two different values of the applies tensile stress σ_0. It is seen that the migrating GB is bent around the inclusion. Also, from Fig. 3, it follows that the GB migration length grows with the increasing applied stress σ_0. When the stress σ_0 reaches its critical value σ_{0c}, the limited GB migration switches to the mode of unlimited migration, in

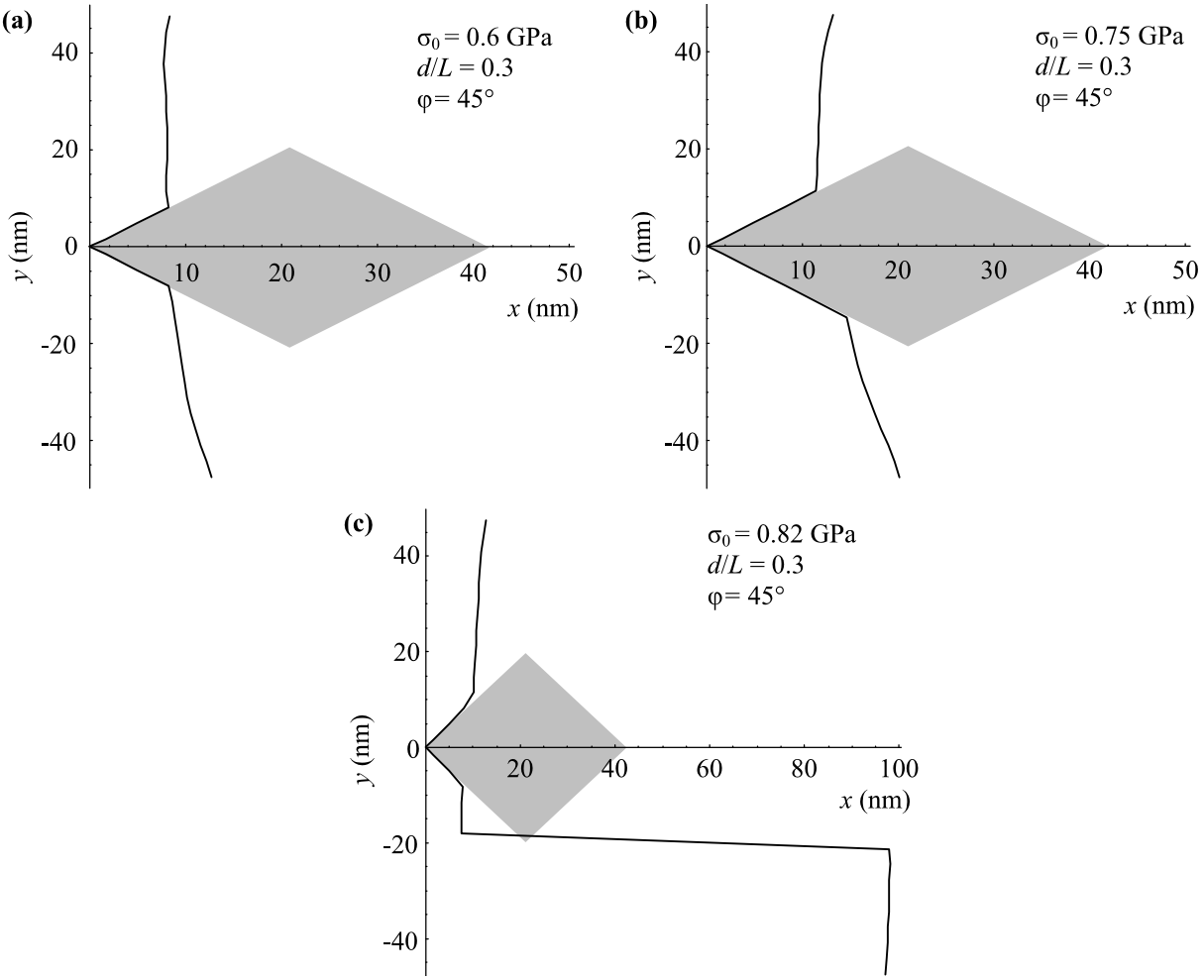

Fig. 4. Geometry of a migrating grain boundary that bends around a nanoinclusion at various values of applied stress calculated for angle φ = 45°. (a), (b) Equilibrium profiles of a migrating grain boundary. (c) Nonequilibrium profile of a migrating grain boundary.

which case the middle segment of the migrating GB is stopped by the nanoinclusion and separates from the upper and lower GB segments that move in the unlimited way (Fig. 3c). In other words, the GB splits into three GB segments. The middle segment is stopped by the inclusion, while the upper and lower segments are mobile. Obviously, the size of the middle GB segment (which is bent around the nanoinclusion) is smaller than the size of the whole migrating GB in Figs. 3a and 3b. Since the characteristic equilibrium migration length of a GB decreases with the decreasing GB length [24], the equilibrium migration length for the middle GB segment is smaller than that for the whole GB. As a result, with time, this GB segment falls back a little toward the initial position of the migrating GB (Fig. 3c). Fig. 3 show moderate asymmetry of the GB profile relative to the GB middle point, which is more pronounced in case of unlimited migration (Fig. 3c). Here we see that upper part (furthest from the crack tip) of the GB moves ahead of bottom part. Asymmetry is obviously caused by non-uniform distribution of stresses in the crack vicinity.

Similarly, Figs. 4a and 4b show the simulated equilibrium profiles of the migrating GB, for d/L = 0.3, φ = 45°. Figs. 4a and 4b demonstrate more pronounced asymmetry of the GB profile than Fig. 3 due to more non-uniform distribution of stress. The case of unlimited migration illustrated in Fig. 4c is even more interesting. Here only bottom part (closest to the crack) switches into unstable migration mode, while upper part remains stable. This behavior is not captured in Fig. 3 due to different stress distribution along migrating GB plane in case of φ = -45°.

Asymmetry of GB profiles was not observed in Ref. [46], where GB migration under uniform load was modeled. As it follows from results of earlier models [53,54], it should not be possible under uniform loading due to simple reasons. Critical stress

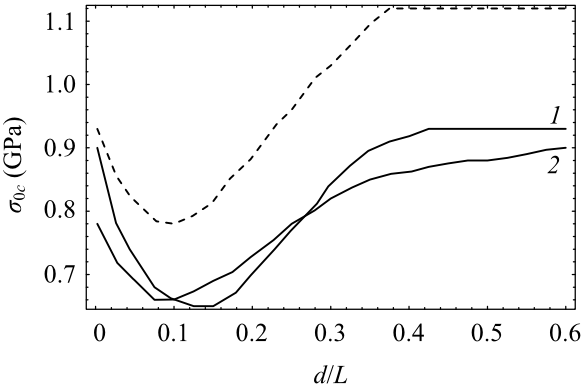

Fig. 5. Dependence of the normalized critical stress σ_{0c} for unlimited migration of a low-angle grain boundary in the vicinity of a crack tip on the ratio *d*/*L* of the nanoinclusion size *d* to the grain boundary length *L* calculated for $\omega = 5°$, $l_{cr} = L$, and angles $\varphi = -45°$ and 45° (curves 1 and 2, respectively). Dashed curve illustrate critical stress σ_{0c} in the absence of a crack (calculated after Ref. [32]).

for transition into unstable migration mode almost exclusively depends on applied stress and misorientation angle [53,54] and independent from GB length. Thus in case of uniform shear stress GB segments not stopped by inclusion should transition into unstable migration mode simultaneously regardless of their length (provided their misorientation is the same). Perturbation induced by crack makes asymmetric transition possible at certain orientations of GB plane relative to crack plane.

As follows from above analysis the transition from limited to unlimited GB migration occurs at some critical applied stress σ_{0c},. We calculated dependence of σ_{0c}, on normalized nanoinclusion size *d*/*L* for $\alpha = 45°$, $\omega = 5°$ and different values of angle $\varphi = -45°$ and $\varphi = 45°$ (curves 1 and 2, respectively). These angles represent certain typical ranges of GB plane orientations relative to axis load producing maximum shear stresses in GB dislocations slip plane. As follows from [46] critical stress is directly proportional to misorientation angle ω, so it is trivial to extend dependences at Fig. 5 to an arbitrary misorientation angle. For comparison dashed line in Fig. 5 shows dependence calculated using results of Ref. [46] in the absence of crack, i.e. under the action of uniform shear stress. Qualitatively dependences of $\sigma_{0c}(d/L)$ are the same as in the absence of crack, so all conclusions made in [46] about character of nanoinclusion size dependence are still valid here. In particular, most important result is that for small values of *d*/*L*, the critical stress decreases with the rise in nanoparticle size *d* (Fig. 5). This means that small nanoparticles can promote migration of low-angle GBs. At the same time, for comparatively large values of *d*/*L*, the critical stress grows with an increase in the ratio *d*/*L*, as one could expect (Fig. 5) and large enough nanoinclusions suppress grain growth. We see that all orientations of GB plane results in lower critical stress σ_{0c} (by about 20%) as should be expected due to stress concentration near crack tip and thus easier transition into unstable migration mode promoting grain growth. The difference between various orientations of GB plane characterized by angle j is minimal (less than 5%).

4. CONCLUSION

To summarize, we proposed a model describing stress-driven migration of low-angle GBs in the vicinity of growing crack in metal matrix nanocomposites with reinforcing (metallic or ceramic) incoherent nanoinclusions. According to the results of our theoretical analysis, this migration can occur in the limited and unlimited modes similar to the model [32?] describing the same process under uniform external load (without crack). In the limited migration mode, migrating GBs eventually approach their equilibrium positions corresponding to a given value of the applied stress (Figs. 3a,b and 4a,b). In the unlimited migration mode, some segments of a migrating GB stop at the nanoinclusion boundary, while others move unrestrictedly far away from the nanoinclusion (Figs. 4c and 5b). The transition from limited to unlimited GB migration occurs at some critical value of the applied stress. This critical stress serves as the key characteristic for the effects exhibited by nanoinclusions on the stress-driven GB migration in nanocomposites. Our analysis demonstrated that in the examined case of a nanocomposite containing nanoinclusions, the critical stress significantly depends on such geometric parameters as the ratio *d*/*L*. This implies that large enough nanoinclusions hinder GB migration. We showed that critical stress in the vicinity of crack always lower than that in the absence of crack as one could expect due to significant stress concentration.

ACKNOWLEDGEMENTS

This work was supported, in part (for SVB), by the Russian Ministry of Education and Science (Zadanie 16.3483.2017/PCh) and the Council for grants of the President of Russian Federation (grant MD-

3154.2017.1), and, in part (for LDG), by the Russian Foundation of Basic Research (grant 17-31-50030).

REFERENCES

[1] E.C. Aifantis // *Mater. Sci. Eng. A* **503** (2009) 190.
[2] M. Dao, L. Lu, R.J. Asaro, J.T.M. De Hosson and E. Ma // *Acta Mater.* **55** (2007) 4041.
[3] J.R. Greer and J.T.M. De Hosson // *Prog. Mater. Sci.* **56** (2011) 654.
[4] M. Kawasaki and T.G. Langdon // *J. Mater. Sci.* **51** (2016) 19.
[5] C.C. Koch, I.A. Ovid'ko, S. Seal and S. Veprek, *Structural Nanocrystalline Materials: Fundamentals and Applications* (Cambridge University Press, Cambridge, 2007).
[6] P. Kumar, M. Kawasaki and T.G. Langdon // *J. Mater. Sci.* **51** (2016) 7.
[7] I.A. Ovid'ko and T.G. Langdon // *Rev. Adv. Mater. Sci.* **30** (2012) 103.
[8] R.Z. Valiev, A.P. Zhilyaev and T.G. Langdon, *Bulk Nanostructured Materials: Fundamentals and Applications* (Wiley, Hoboken, New Jersey, USA, 2014).
[9] R.Z. Valiev and Y.T. Zhu // *Trans. MRS Japan* **40** (2015) 309.
[10] Y.T. Zhu, X.Z. Liao and X.L. Wu // *Prog. Mater. Sci.* **57** (2012) 1.
[11] S.V. Bobylev, N.F. Morozov and I.A. Ovid'ko // *Phys. Rev. Lett.* **105** (2010) 055504.
[12] S.V. Bobylev, N.F. Morozov and I.A. Ovid'ko // *Phys. Rev. B* **84** (2011) 094103.
[13] S.V. Bobylev, N.F. Morozov and I.A. Ovid'ko // *Rev. Adv. Mater. Sci.* **48** (2017) 131.
[14] S.V. Bobylev, N.F. Morozov and I.A. Ovid'ko // *Dokl. Phys.* **62** (2017) 124.
[15] S.V. Bobylev and I.A. Ovid'ko // *Phys. Rev. Lett.* **109** (2012) 175501.
[16] S.V. Bobylev and I.A. Ovid'ko // *Acta Mater.* **88** (2015) 260.
[17] S.V. Bobylev and I.A. Ovid'ko // *Acta Mater.* **124** (2017) 333.
[18] S.V. Bobylev and I.A. Ovid'ko // *Rev. Adv. Mater. Sci.* **50** (2017) 104.
[19] J.T.M. De Hosson, W.A. Soer, A.M. Minor, Z.W. Shan, E.A. Stach, S.A. Syed Asif and O.L. Warren // *J. Mater. Sci.* **41** (2006) 7704.
[20] V. Dupont and F. Sansoz // *Acta Mater.* **56** (2008) 6013.
[21] D. Farkas, A. Frřseth and H. Van Swygenhoven // *Scr. Mater.* **55** (2006) 695.
[22] D.S. Gianola, S. Van Petegem, M. Legros, S. Brandstetter, H. Van Swygenhoven and K.J. Hemker // *Acta Mater.* **54** (2006) 2253.
[23] D.S. Gianola, D.H. Warner, J.F. Molinari and K.J. Hemker // *Scr. Mater.* **55** (2006) 649.
[24] M.Y. Gutkin and I.A. Ovid'ko // *Appl. Phys. Lett.* **87** (2005) 251916.
[25] M. Jin, A.M. Minor, E.A. Stach and J.W. Morris // *Acta Mater.* **52** (2004) 5381.
[26] X.Z. Liao, A.R. Kilmametov, R.Z. Valiev, H.S. Gao, X.D. Li, A.K. Mukherjee, J.F. Bingert and Y.T. Zhu // *Appl. Phys. Lett.* **88** (2006) 021909.
[27] Y.J. Lin, H.M. Wen, Y. Li, B. Wen, W. Liu and E.J. Lavernia // *Acta Mater.* **82** (2015) 304.
[28] I.A. Ovid'ko and A.G. Sheinerman // *Rev. Adv. Mater. Sci.* **39** (2014) 99.
[29] I.A. Ovid'ko and A.G. Sheinerman // *J. Mater. Sci.* **50** (2015) 4430.
[30] I.A. Ovid'ko, A.G. Sheinerman and E.C. Aifantis // *Acta Mater.* **59** (2011) 5023.
[31] I.A. Ovid'ko and A.G. Sheinerman // *Acta Mater.* **121** (2016) 117.
[32] I.A. Ovid'ko, A.G. Sheinerman and E.C. Aifantis // *Acta Mater.* **56** (2008) 2718.
[33] F. Sansoz and V. Dupont // *Appl. Phys. Lett.* **89** (2006) 111901.
[34] J.A. Sharon, P.-C. Su, F.B. Prinz and K.J. Hemker // *Scr. Mater.* **64** (2011) 25.
[35] W.A. Soer, J.T.M. De Hosson, A.M. Minor, J.W. Morris and E.A. Stach // *Acta Mater.* **52** (2004) 5783.
[36] P.R. Rios // *Acta Metall*. **35** (1987) 2805.
[37] P.A. Manohar, M. Ferry and T. Chandra // *ISIJ International* **38** (1998) 913.
[38] G.-H. Kim, S.-M.Hong, M.-K. Lee, S.-H. Kim, I. Ioka, B.-S. Kim and I.-S. Kim // *Mater. Trans. A* **51** (2010) 1951.
[39] J.F. Guo, J. Lio, C.N. Sun, S. Maleksaeedi, G. Bi, M.J. Tan and J. Wei // *Mater. Sci. Eng. A* **602** (2014) 143.
[40] N. Abdolrahim, I.N. Mastorakos and H.M. Zbib // *Philos. Mag. Lett.* **92** (2012) 597.
[41] S. Torizuka, E. Muramatsu, S.V.S. Narayana Murty and K. Nagai // *Scr. Mater.* **55** (2006) 751.
[42] H. Askari, H. Zbib and X. Sun // *J. Nanomech. Micromech.* **3** (2013) 24.
[43] D.L. Davidson // *Composites* **24** (1993) 248.
[44] H. Feng, Y. Zhou, J. Dechang and M. Qingchang // *Comp. Sci. Technol.* **64** (2004) 2495.

[45] J. Li, Q. Fang and Y. Liu // *Int. J. Engn. Sci.* **72** (2013) 89.
[46] I.A. Ovid'ko and A.G. Sheinerman // *J. Mater. Sci.* **50** (2015) 4430.
[47] M. Ke, W.W. Milligan, S.A. Hackney, J.E. Carsley and E.C. Aifantis // *Nanostruct. Mater*. **5** (1995) 689.
[48] Z. Shan, J.A. Knapp, D.M. Follstaedt, E.A. Stach, J.M.K. Wiezorek and S.X. Mao // *Phys. Rev. Lett.* **100** (2008) 105502.
[49] S. Cheng, Y. Zhao, Y. Wang, Y. Li, X.-L. Wang, P.K. Liaw and E.J. Lavernia // *Phys. Rev. Lett.* **104** (2010) 255501.
[50] P. Liu, S.C. Mao, L.H. Wang, X.D. Han and Z. Zhang // *Scr. Mater.* **64** (2011) 343.
[51] S. Cheng, S.Y. Lee, L. Li, C. Lei, J. Almer, X.-L. Wang, T. Ungar, Y. Wang and P.K. Liaw // *Phys. Rev. Lett.* **110** (2013) 135501.
[52] A.P. Sutton and R.W. Balluffi, *Interfaces in Crystalline Materials* (Oxford Science Publications, Oxford, 1996).
[53] S.V. Bobylev, M.Yu. Gutkin and I.A. Ovid'ko // *J. Phys. D* **37** (2004) 269.
[54] S.V. Bobylev, M.Yu. Gutkin and I.A. Ovid'ko // *Acta Mater.* **52** (2004) 3793.
[55] E.A. Rzhavtsev and M.Yu. Gutkin // *Scr. Mater.* **100** (2015) 102.
[56] S.V. Bobylev and I.A. Ovid'ko // *Acta Mater.* **88** (2015) 260.
[57] *Fracture Mechanics and Strength of Materials, vol. 2*, ed. by V.V. Panasyuk (Naukova Dumka, Kiev, 1988), In Russian.
[58] A.Yu. Kuksin and A.V. Yanilkin // *Phys. Sol. State* **55** (2013) 1010.